Published in final edited form as:
Nat Struct Mol Biol. 2016 July ; 23(7): 624–630. doi:10.1038/nsmb.3244.

Towards the atomic structure of the Nuclear Pore Complex: When top down meets bottom up

André Hoelz[1,*], **Joseph S. Glavy**[2,*], and **Martin Beck**[3,*]

[1]Division of Chemistry and Chemical Engineering, California Institute of Technology, 1200 East California Boulevard, Pasadena, CA 91125, USA

[2]Department of Chemistry, Chemical Biology and Biomedical Engineering, Stevens Institute of Technology, 507 River Street, Hoboken, NJ 07030, USA

[3]European Molecular Biology Laboratory, Structural and Computational Biology Unit, Meyerhofstrasse 1, 69117 Heidelberg, Germany

Abstract

Elucidating the structure of the nuclear pore complex (NPC) is a prerequisite for understanding the molecular mechanism of nucleocytoplasmic transport. However, due to sheer size and flexibility, the NPC is unapproachable by classical structure determination techniques and requires a joint effort of complementary methods. Whereas bottom up approaches rely on biochemical interaction studies and crystal structure determination of NPC components, top down approaches attempt to determine the structure of the intact NPC *in situ*. Recently, both approaches have converged, bridging the resolution gap from higher-order scaffold structure to near-atomic resolution and opening the door for structure-guided experimental interrogations of NPC function.

The nuclear pore complex (NPC) is one of the largest proteinaceous assemblies in eukaryotic cells, forming a mega-Dalton transport channel embedded in the nuclear envelope that mediates the bidirectional exchange of macromolecules between the nucleus and cytoplasm. In addition to their critical role in nucleocytoplasmic trafficking, NPCs participate in a variety of key cellular processes, and are essential for eukaryotic life (reviewed e.g. in [1]). Structural information is fundamental for understanding the molecular mechanisms of nucleocytoplasmic transport, because the spatial organization of NPC components ultimately determines how cargos cross its permeability barrier. However, the NPC structure has long remained elusive, largely because of its sheer size, inherent flexibility, and membrane embedded nature that renders it inaccessible for well-established structure determination approaches. Based on the observation that NPCs assemble from biochemically stable sub-complexes, an alternative divide-and-conquer approach has been pursued for more than a decade. With this strategy, the NPC is divided into relatively smaller, more manageable sub-complexes for X-ray crystallographic studies with the hope that the resulting crystal structures could eventually be fitted into a three-dimensional electron microscopic reconstruction of the intact NPC [1,2]. Yet, an impediment specific to NPCs and other mega assemblies is the existence of a higher-order scaffold structure with an

*Correspondence: hoelz@caltech.edu (A.H.), jglavy@stevens.edu (J.G.), martin.beck@embl.de (M.B.).

organizational level that goes beyond the quaternary structure of a single sub-complex, and includes how sub-complexes interact with multiple copies of themselves and other sub-complexes. Recent work from several laboratories has now enabled the placement of the first piece of this huge molecular puzzle, demonstrating the feasibility of this approach and foreshadowing the elucidation of the entire NPC structure in the near future [3,4]. Here, we discuss how this has been achieved by the combination of two complementary approaches, bottom up *in vitro* and top down *in situ* structural biology, which have now converged and generated the first predictive structural models of the nuclear pore scaffold.

Structural analysis of the Y-complex in vitro

NPCs have an outer diameter of ~120 nm and a molecular mass of ~110 MDa, which corresponds to about 1 million residues (~10 million non-hydrogen atoms). Over the last half-century, electron microscopic studies have established that NPCs possess a symmetric core with eight-fold and pseudo two-fold rotational symmetry along the nucleocytoplasmic axis and the plane of the nuclear envelope, respectively (reviewed in [1]) (Figure 1A). These studies also morphologically defined the three main substructures of the NPC that engage with the fused membranes: outer cytoplasmic and nuclear rings, which sandwich a third inner ring (also referred to as the spoke ring). Proteomic approaches in yeast and human cells have revealed that NPCs are composed of an evolutionarily conserved set of just over 30 different proteins, collectively termed nucleoporins (Nups) [5,6]. Traditionally, nucleoporins have been named according to their molecular mass, and as such a unified nomenclature does not exist due to the surprising variability in mass between nucleoporin orthologs from different species (reviewed in [1,2]). However, based on their approximate location within the NPC, nucleoporins can be classified into six categories: (1) coat nucleoporins, (2) transmembrane nucleoporins (also called pore membrane proteins, POMs), (3) adaptor nucleoporins, (4) channel nucleoporins, (5) cytoplasmic filament nucleoporins, and (6) nuclear basket nucleoporins [1,7] (Table 1, Figure 1A). Here, we will focus on the elucidation of the higher-order scaffold structure of the coat nucleoporins that form the two outer rings of the NPC.

Composition of the nuclear pore

Despite its large and extended structure, the components of the coat nucleoporin complex (CNC) tightly interact with each other, which allowed for its intact biochemical isolation from yeast and human cells more than a decade ago [8–11]. This analysis yielded a hetero-heptameric and a hetero-decameric complex from yeast and human cells, respectively (also denoted Nup84 and Nup107 sub-complexes according to one of their components), suggesting that the coat nucleoporins Nup120, Seh1, Nup85, Sec13, Nup145C, Nup84, and Nup133 form an evolutionarily conserved core (Fig. 1B and Table 1) that is complemented with three additional proteins, Nup37, Nup43, and Elys in human cells (Figure 2A) [12]. However, recent reconstitutions of CNCs from the thermophilic eukaryotes *Chaetomium thermophilum* and *Myceliophthora thermophila* both lacked Seh1, suggesting a smaller evolutionarily conserved core composed of only six coat nucleoporins [13,14]. Regardless of composition, negative-stain EM analyses have established that the coat nucleoporin complex (CNC) adopts an extended Y-shaped structure (inspiring its designation as the “Y complex”)

that is evolutionarily conserved across all organisms analyzed to date[3,13,15,16]. Biochemical reconstitution experiments established that the entire CNC can be assembled in the test tube by mixing purified recombinant *S. cerevisiae* or *C. thermophilum* coat nucleoporins [13,17].

X-ray crystallographic analyses of the coat nucleoporins of the Y-shaped CNC began about a decade ago, yielding more than ten crystal structures in short intervals, starting with the N-terminal Nup133 β-propeller domain, followed by the interaction between the C-terminal α-helical domains of Nup107 (yNup84) and Nup133, the Sec13•Nup145C pair, the Seh1•Nup85 hetero-dimer, the Nup120 N-terminal domain, the Sec13•Nup145C•Nup84 hetero-trimer, and finally the entire C-terminal α-helical solenoid of Nup133 [7,18–26] In initial attempts to understand the connectivity of the Y-complex, these small pieces of the puzzle were oriented to each other based on a three-dimensional map obtained by negative-staining electron microscopy and random conical tilt reconstruction [27], where 3D reconstructions were calculated from electron micrographs that contain the single particles in preferred orientation but are acquired at different tilt angles. Despite a limited resolution of ~35 Å, this map allowed for the approximate fitting of the individual crystal structures, providing a first glimpse into the structure of the entire complex [25] (Figure 1C).

Electron microscopic analysis of nuclear pores in situ

These findings prompted questions about how subcomplexes interact with each other *in situ.* To study the higher order assembly of subcomplexes within the fully assembled nuclear pore different, complementary approaches are required. Several laboratories have investigated the structure of the entire NPC with cryo-EM. Initial reconstructions of the *Xenopus* and yeast NPCs were obtained in part from extracted and purified samples. The resulting maps suffered to varying degrees from non-isotropic resolution due to angular coverage problems of the primary data. Due to the prevalence of ‘top views’ in the primary data structural features along the nucleocytoplamic axis appeared elongated and distorted. This resulted in an overall donut-shaped layout that was, to some extent, reflected in early models of the higher-order scaffold structure NPC [7,20,28–31]. This layout was devoid of the clear morphological separation into the nuclear, cytoplasmic and inner rings seen by tomographic reconstructions of the NPC from intact *Dictyostelium* nuclei and human cells [32–34] that had addressed the angular coverage problems. Due to the relatively low resolution, the resulting cryo-EM maps were still devoid of any Y-shaped features. This was also true of the *Dictyostelium* NPC reconstruction, which at ~58 Å possessed the highest resolution of any of the maps. The field’s inability to relate the high-resolution coat nucleoporin crystal structures to the overall NPC was not only frustrating, it also lead to a rigorous debate about the stoichiometry and arrangement of the CNC within the intact NPC scaffold [7,20,31].

Convergence of top-down in situ and bottom up in vitro approaches

Two key structural challenges had to be overcome in order to resolve this riddle. First, a higher resolution EM reconstruction of the intact NPC was needed to allow for confident fitting of coat nucleoporin crystal structures. This was achieved by the Beck and Glavy groups, who employed an integrated structural analysis by cryo electron tomography of the human NPC [3]. In addition to acquiring a tomographic map of the entire NPC, this study also

obtained a negative-staining EM reconstruction of the human CNC (Figure 1D), both were determined by subtomogram averaging at resolutions of ~32 Å. Facilitated by the higher resolution, the human CNC EM reconstruction could be fitted into 32 positions within the cytoplasmic and nuclear rings that had simply been unresolved in previous reconstructions (Figure 1E). This and two subsequent studies used an unbiased fitting procedure that systematically explores the tomographic map with a given nucleoporin or entire sub-complex, exhausting all possible placements and conformations [3,4,35]. In this way, tens of thousands of possible solutions are scored for agreement with the tomographic map. The best possible fits are then objectively compared to alternative solutions. Though this approach can be used regardless of the quality of the tomographic map, the statistical discrimination between the different fits will naturally be stronger with higher resolution. Similarly, employing larger nucleoporin structures provides more data points on the virtual grid to be compared, resulting in a more statistically significant fitting.

In contrast to earlier conceptual models [1], 32 copies of the CNC assembled into two eight-membered concentric rings on both the cytoplasmic and nuclear faces of the NPC. With this new map, the available structures of individual coat nucleoporins could be roughly positioned within the cryo-EM map based on their fit into the negative-stain EM reconstruction of the human CNC. However, because the negative-stain EM reconstruction of the CNC was itself limited in resolution, the exact orientation of coat nucleoporins within the context of the intact NPC remained elusive. Moreover, a crystal structure of the central triskelion—the critically important central CNC element that joins the three arms of the Y complex—was still missing from the nucleoporin structural inventory.

This second set of challenges has now also been met. A recent study by the Hoelz group determined the crystal structure of the intact yeast CNC lacking only the loosely associated Nup133. This was achieved with the help of a high-affinity conformation-specific antibody that recognized the fully assembled CNC [4] (Figure 1B). This ~400 kDa CNC crystal structure revealed the molecular details of how the three arms of the Y interact within the central triskelion. The structure of the CNC was determined using crystals with two different crystal-packing arrangements, both of which yielded identical structures. Despite good agreement with the negative staining structures, the crystal structures revealed an overall more curved Y-shaped conformation (Figure 1C, D). Importantly, the yeast CNC crystal structure allowed for the unbiased, systematic fitting into the cryo-EM reconstruction of the intact human NPC. This approach yielded 32 copies of the CNC arranged in four rings, not only confirming the arrangement proposed by the Beck and Glavy groups, but also directly bridging the resolution gap between tomographic reconstructions and X-ray crystallography studies for the first time. This advance established the near-atomic structure of the NPC coat and demonstrated that the divide-and-conquer approach proposed more than a decade ago is feasible and will likely enable the elucidation of the near-atomic structure of the intact NPC.

At the same time, the Schwartz group used a different approach to obtain an atomic model of the intact CNC. The crystal structure of the central triskelion alone, truncated to the minimal fragments, was solved using proteins from the eukaryotic thermophile *Myceliophthora thermophila* [14]. Based on components of the central hub that overlapped with existing crystal structures, a composite model of the entire complex was generated *in*

silico. This approach yielded a considerably different conformation than was observed in the crystal structure of the intact CNC (lacking Nup133) [4]. Specifically, a substantially different angle between the stalk and one of the upper arms of the CNC was observed. Consequently, the *Myceliophthora* structure cannot be successfully fitted into negative-stain EM reconstructions of the yeast or human CNCs. Similarly, this modeled conformation cannot be fitted into the tomographic map of the intact human NPC without causing clashes [14]. Conformational differences in CNC curvature are also apparent when the crystal structure of the intact CNC [4] is compared to the overall flatter negative staining CNC EM structure (Figure 1D) – although the deviations are much less pronounced in the latter [3,4]. However, as mentioned above a striking conformational agreement is clearly evident when the crystal structure of the intact CNC [4] is compared to tomographic maps [3], likely because both X-ray crystallography and electron microscopy structure determination approaches selected for the energetically most favorable conformations [3,4,35]. Since fully assembled NPCs are dynamic structures, the observed conformational differences could be due to inherent flexibility. Future work will be needed to address whether such conformational flexibility of the CNC holds any physiologic relevance [33,36].

Composite structures of the nuclear pore scaffold

Most recently, the Beck and Glavy groups published a tomographic reconstruction of the intact human NPC that was obtained using direct electron detection (Figure 2B). Although the map boasts an overall resolution of up to ~23 Å, the local resolution varies and is generally higher for the more defined scaffold domains and a little lower at the peripheral regions of the NPC [3]. The increased resolution of this reconstruction was achieved not only by employing a direct electron detector, but also by improving data acquisition and image processing procedures that allow for the collection of larger datasets and account for the intrinsic flexibility of the NPC subdomains. Specifically, image processing did not assume a strict eight-fold-rotational symmetry but rather allowed for asymmetric units (rotational segments) to be aligned independently. Additionally, the three different nuclear, inner, and cytoplasmic NPC rings were refined independently to account for conformational plasticity.

The sixteen-membered, double-ring CNC arrangement is apparent on both the cytoplasmic and nuclear faces of the NPC, although their structures were solved independently and are non-identical due to differential binding of peripheral nucleoporins. The shapes of several key domains of the CNC rings, such as the β-propeller domains of the coat nucleoporins, are obvious at the improved resolution, further confirming the previous CNC positioning [3,4,35]. Several individual crystal structures of the CNC could thus be directly fitted into the tomographic map, yielding a hybrid structure that imposes very well with the crystal structure of the hexameric CNC obtained by the Hoelz group (Figure 2C–E). Although the positioning of the smaller crystal structures is often aided by complementary interaction data, the precise orientations of multiple coat nucleoporins still needs to be refined. For example, although additional density explaining the disc-shaped β-propeller domain of Elys is detected proximal to its biochemically defined binding site on Nup160, the rotation of this domain around its central axis cannot be determined at the current resolution. Obtaining crystal structures that resolve these interactions will be one way to address these types of uncertainties in the future.

The Schwartz group has argued that the tomographic map might represent and overlay of two alternative stem conformations of only 8 Y-complexes (CNC) within each the cytoplasmic and nuclear rings [14]. Kelley et al. argue that these two hypothetical conformations differ the stem region of the CNC but overlay in its branching region that contains the central hub. However, if the topographic map would be an average of two considerably different conformational populations, this would not only disturb the alignment of subtomograms and massively reduce the attainable resolution. More importantly, if the stem regions were contained in alternative conformations, then the respective electron optical density would appear significantly weaker or 'diluted' when compared to other static features in the NPC, such is the neighboring central hub of the CNC. However, this was not observed in the reconstruction and can clearly be seen when the density of the stem and central hub are compared. Also the inner and outer CNC rings display an intensity that is consistent with other features of the scaffold, clearly ruling out this interpretation. Additional work has since provided further support for the sixteen-membered cytoplasmic and nucleoplasmic CNC double-ring arrangement. For example, gene silencing of Nup358 in mammalian cells results in a specific loss of the distal (outer) CNC ring solely on the cytoplasmic face (Figure 3), while not affecting the double CNC ring arrangement at the nuclear face [35]. Image classification of the respective data recovered the distal CNC in about 5% of the subunits, in line with the knock-down efficiency. Since this approach recovers structural information from individual subunits, it is obviously independent from the 8-fold rotational symmetry [35], other than argued by the Schwartz group [14]. Further, super-resolution microscopy approaches have confirmed the stoichiometry and orientation of the Y complex, proximity labeling has provided evidence for some of the respective interactions, and the electron density of a recent cryo-EM reconstruction of the *Xenopus laevis* NPC also contained the double CNC ring arrangement. Jointly, the overall model illustrated in Figure 4 [37–40] is supported.

Clearly, much remains to be done to uncover the structure of the nuclear pore at side chain resolution. With the advent of recent EM breakthroughs, it is likely that the resolution limit has not yet been reached. Further technological improvements may facilitate the acquisition of reconstructions pushing the resolution beyond ~10 Å, which would reveal nucleoporin secondary structure elements and allow for more accurate crystal structure positioning using flexible fitting approaches. To achieve this goal, the crystal structures of all remaining ordered nucleoporins need to be determined. Important steps towards this goal have been the recently determined crystal structures of the fungal Nsp1•Nup49•Nup57 channel nucleoporin heterotrimer (CNT; also termed Nsp1 or Nup62 complex) and its vertebrate homolog [41,42]. The fungal structure also visualized the interaction between the CNT and the adaptor nucleoporin Nic96, revealing how the pore is able to select for a single defined CNT assembly state to be incorporated into the NPC scaffold [41]. Additionally, the reconstitution of a ~550 kDa complex containing the inner ring and cytoplasmic filament nucleoporin complexes from purified recombinant proteins, not only yielded the largest nucleoporin complex reconstituted to date, but its systematic biochemical dissection also revealed the detailed underlying nucleoporin-nucleoporin interaction network and identified architecturally important nucleoporin interactions that are currently missing from our crystal structure inventory [41,43]. These data have in the meantime been integrated into a

comprehensive composite structure of the inner ring complex (Lin et al; Kosinski et al, SCIENCE to appear 15th of April). Taken together, the vast majority of the electron optical density observed *in situ* is now accounted by high-resolution crystal structures of scaffold nucleoporins.

Future directions for the structure determination of the nuclear pore

An atomic resolution composite structure of the NPC is highly desirable for many reasons. First, although the major constituents of the permeability barrier within the NPC are intrinsically disordered regions that will remain elusive to present structure determination technologies, it is the folded scaffold nucleoporins that define the position of these regions by anchoring them to specific locations in the central channel. Thus, knowledge of the precise arrangement of the scaffold is essential to define the local concentrations and stoichiometry of intrinsically disordered transport channel domains. This is a key prerequisite for computer simulations and *in vitro* reconstitution experiments that aim to understand how a different local biophysical environment within the central channel facilitates the interaction with specific cargo complexes and eventually direct them through the channel efficiently. Second, structure-guided site-directed mutagenesis studies, which remain underexplored in the NPC field due to the lack of structural information, will be crucial to validate functional hypotheses for nucleo-cytoplasmic transport. Although the structured nucleoporins are believed to be less important during the actual transport of cargo, they likely play an important role in various fundamental biological processes, including the mechanisms of nuclear import of integral membrane proteins, export, remodeling and sorting of messenger ribonucleoprotein (mRNPs), NPC assembly and disassembly, NPC-associated DNA repair and transcription events, and many more. Finally and perhaps most importantly, a composite structure of the NPC would facilitate the elucidation of the molecular basis for nucleoporin related health conditions, such as cancer and the loss of integrity of the permeability barrier during aging, opening the door for the development of novel treatments.

The recent series of advances constitute major steps towards the elucidation of the higher-order scaffold structure of the NPC. After more than a decade of concentrated efforts, two sub-communities of the NPC field employing two vastly different approaches—the top down *in situ* and the bottom up *in vitro* approach—finally meet in the middle. With this advance, structural models of the NPC have become predictive and experimentally testable, which is an important milestone. Following the successful placement of the CNC, a keystone piece in the intricate three-dimensional NPC puzzle, we expect that adding the remaining pieces will be achieved in the near future.

Acknowledgments

We thank Alina Patke for critical reading of the manuscript and Alexander von Appen and Jan Kosinski for help with preparing the figures. A.H. is an inaugural Heritage Principal Investigator of the Heritage Research Institute for the Advancement of Medicine and Science at Caltech and was supported by Caltech startup funds, the Albert Wyrick V Scholar Award of the V Foundation for Cancer Research, the 54th Mallinckrodt Scholar Award of the Edward Mallinckrodt Jr. Foundation, a Kimmel Scholar Award of the Sidney Kimmel Foundation for Cancer Research, a Camille-Dreyfus Teacher Scholar Award of The Camille & Henry Dreyfus Foundation, and National Institutes of Health (NIH) grants R01-GM111461 and R01-GM117360. J.S.G. was supported by National Institute

on Aging (NIA) grant R21-AG047433. M.B. acknowledges funding by the EMBL and the European Research Council (309271-NPCAtlas).

References

1. Hoelz A, Debler EW, Blobel G. The Structure of the Nuclear Pore Complex. Annu Rev Biochem. 2011; 80:613–643. [PubMed: 21495847]
2. Schwartz TU. Modularity within the architecture of the nuclear pore complex. Curr Opin Struct Biol. 2005; 15:221–6. [PubMed: 15837182]
3. Bui KH, et al. Integrated structural analysis of the human nuclear pore complex scaffold. Cell. 2013; 155:1233–43. [PubMed: 24315095]
4. Stuwe T, et al. Nuclear pores. Architecture of the nuclear pore complex coat. Science. 2015; 347:1148–52. [PubMed: 25745173]
5. Cronshaw JM, Krutchinsky AN, Zhang W, Chait BT, Matunis MJ. Proteomic analysis of the mammalian nuclear pore complex. J Cell Biol. 2002; 158:915–27. [PubMed: 12196509]
6. Rout MP, et al. The yeast nuclear pore complex: composition, architecture, and transport mechanism. J Cell Biol. 2000; 148:635–51. [PubMed: 10684247]
7. Hsia KC, Stavropoulos P, Blobel G, Hoelz A. Architecture of a coat for the nuclear pore membrane. Cell. 2007; 131:1313–26. [PubMed: 18160040]
8. Siniossoglou S, et al. Structure and assembly of the Nup84p complex. J Cell Biol. 2000; 149:41–53. [PubMed: 10747086]
9. Loiodice I, et al. The entire Nup107–160 complex, including three new members, is targeted as one entity to kinetochores in Mitosis. Mol Biol Cell. 2004; 15:3333–3344. [PubMed: 15146057]
10. Walther TC, et al. The conserved Nup107–160 complex is critical for nuclear pore complex assembly. Cell. 2003; 113:195–206. [PubMed: 12705868]
11. Siniossoglou S, et al. A novel complex of nucleoporins, which includes Sec13p and a Sec13p homolog, is essential for normal nuclear pores. Cell. 1996; 84:265–75. [PubMed: 8565072]
12. Hurt E, Beck M. Towards understanding nuclear pore complex architecture and dynamics in the age of integrative structural analysis. Curr Opin Cell Biol. 2015; 34:31–38. [PubMed: 25938906]
13. Thierbach K, et al. Protein interfaces of the conserved Nup84 complex from Chaetomium thermophilum shown by crosslinking mass spectrometry and electron microscopy. Structure. 2013; 21:1672–82. [PubMed: 23954503]
14. Kelley K, Knockenhauer KE, Kabachinski G, Schwartz TU. Atomic structure of the Y complex of the nuclear pore. Nat Struct Mol Biol. 2015; 22:425–31. [PubMed: 25822992]
15. Flemming D, Thierbach K, Stelter P, Bottcher B, Hurt E. Precise mapping of subunits in multiprotein complexes by a versatile electron microscopy label. Nat Struct Mol Biol. 2010; 17:775–8. [PubMed: 20512149]
16. Kampmann M, Blobel G. Three-dimensional structure and flexibility of a membrane-coating module of the nuclear pore complex. Nat Struct Mol Biol. 2009; 16:782–8. [PubMed: 19503077]
17. Lutzmann M, Kunze R, Buerer A, Aebi U, Hurt E. Modular self-assembly of a Y-shaped multiprotein complex from seven nucleoporins. EMBO J. 2002; 21:387–97. [PubMed: 11823431]
18. Berke IC, Boehmer T, Blobel G, Schwartz TU. Structural and functional analysis of Nup133 domains reveals modular building blocks of the nuclear pore complex. J Cell Biol. 2004; 167:591–7. [PubMed: 15557116]
19. Boehmer T, Jeudy S, Berke IC, Schwartz TU. Structural and functional studies of Nup107/Nup133 interaction and its implications for the architecture of the nuclear pore complex. Mol Cell. 2008; 30:721–31. [PubMed: 18570875]
20. Brohawn SG, Leksa NC, Spear ED, Rajashankar KR, Schwartz TU. Structural evidence for common ancestry of the nuclear pore complex and vesicle coats. Science. 2008; 322:1369–73. [PubMed: 18974315]
21. Debler EW, et al. A fence-like coat for the nuclear pore membrane. Mol Cell. 2008; 32:815–26. [PubMed: 19111661]

22. Leksa NC, Brohawn SG, Schwartz TU. The structure of the scaffold nucleoporin Nup120 reveals a new and unexpected domain architecture. Structure. 2009; 17:1082–91. [PubMed: 19576787]
23. Seo HS, et al. Structural and functional analysis of Nup120 suggests ring formation of the Nup84 complex. Proc Natl Acad Sci USA. 2009; 106:14281–6. [PubMed: 19706512]
24. Brohawn SG, Schwartz TU. Molecular architecture of the Nup84-Nup145C-Sec13 edge element in the nuclear pore complex lattice. Nat Struct Mol Biol. 2009; 16:1173–7. [PubMed: 19855394]
25. Nagy V, et al. Structure of a trimeric nucleoporin complex reveals alternate oligomerization states. Proc Natl Acad Sci USA. 2009; 106:17693–8. [PubMed: 19805193]
26. Whittle JR, Schwartz TU. Architectural nucleoporins Nup157/170 and Nup133 are structurally related and descend from a second ancestral element. J Biol Chem. 2009; 284:28442–52. [PubMed: 19674973]
27. Kampmann M, Blobel G. Three-dimensional structure and flexibility of a membrane-coating module of the nuclear pore complex. Nat Struct Mol Biol. 2009; 16:782–8. [PubMed: 19503077]
28. Akey CW. Interactions and structure of the nuclear pore complex revealed by cryo-electron microscopy. J Cell Biol. 1989; 109:955–70. [PubMed: 2768344]
29. Hinshaw JE, Carragher BO, Milligan RA. Architecture and design of the nuclear pore complex. Cell. 1992; 69:1133–41. [PubMed: 1617726]
30. Yang Q, Rout MP, Akey CW. Three-dimensional architecture of the isolated yeast nuclear pore complex: functional and evolutionary implications. Mol Cell. 1998; 1:223–34. [PubMed: 9659919]
31. Alber F, et al. The molecular architecture of the nuclear pore complex. Nature. 2007; 450:695–701. [PubMed: 18046406]
32. Beck M, et al. Nuclear pore complex structure and dynamics revealed by cryoelectron tomography. Science. 2004; 306:1387–90. [PubMed: 15514115]
33. Beck M, Lucic V, Forster F, Baumeister W, Medalia O. Snapshots of nuclear pore complexes in action captured by cryo-electron tomography. Nature. 2007; 449:611–5. [PubMed: 17851530]
34. Maimon T, Elad N, Dahan I, Medalia O. The Human Nuclear Pore Complex as Revealed by Cryo-Electron Tomography. Structure. 2012; 20:998–1006. [PubMed: 22632834]
35. von Appen A, et al. In situ structural analysis of the human nuclear pore complex. Nature. 2015; 526:140–3. [PubMed: 26416747]
36. Akey CW. Structural plasticity of the nuclear pore complex. J Mol Biol. 1995; 248:273–93. [PubMed: 7739040]
37. Ori A, et al. Cell type-specific nuclear pores: a case in point for context-dependent stoichiometry of molecular machines. Mol Syst Biol. 2013; 9:648. [PubMed: 23511206]
38. Szymborska A, et al. Nuclear pore scaffold structure analyzed by super-resolution microscopy and particle averaging. Science. 2013; 341:655–8. [PubMed: 23845946]
39. Kim DI, et al. Probing nuclear pore complex architecture with proximity-dependent biotinylation. Proc Natl Acad Sci USA. 2014; 111:E2453–61. [PubMed: 24927568]
40. Eibauer M, et al. Structure and gating of the nuclear pore complex. Nat Commun. 2015; 6:7532. [PubMed: 26112706]
41. Stuwe T, et al. Architecture of the fungal nuclear pore inner ring complex. Science. 2015; 350:56–64. [PubMed: 26316600]
42. Chug H, Trakhanov S, Hulsmann BB, Pleiner T, Gorlich D. Crystal structure of the metazoan Nup62*Nup58*Nup54 nucleoporin complex. Science. 2015; 350:106–10. [PubMed: 26292704]
43. Fischer J, Teimer R, Amlacher S, Kunze R, Hurt E. Linker Nups connect the nuclear pore complex inner ring with the outer ring and transport channel. Nat Struct Mol Biol. 2015; 22:774–81. [PubMed: 26344569]

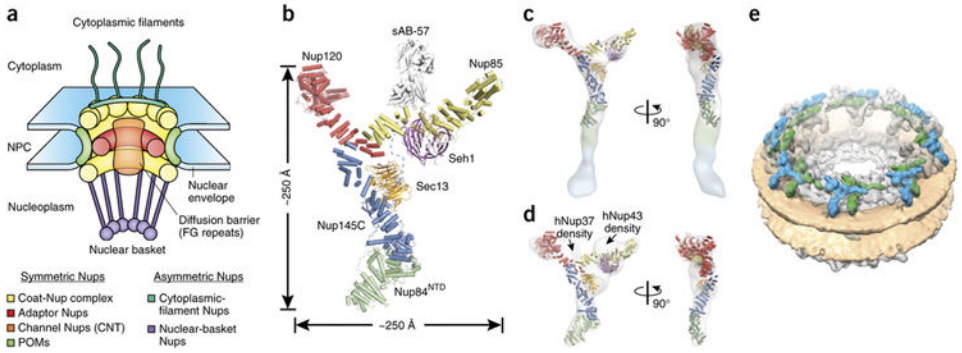

Figure 1. General organization principles of nuclear pores and the Y-shaped coat nucleoporin complex (CNC)

(**a**) Spatial organization of nucleoporin classes as listed in Table 1 (adapted from reference [4]). (**b**) Crystal structure of the fully assembled *S. cerevisiae* CNC [4] shown in cartoon representation (PDB ID 4XMM; lacking Nup133). The CNC crystal structure revealed the overall conformation of the CNC and the molecular details of how the three different arms of the Y-shaped CNC form the central triskelion. The conformation-specific high-affinity synthetic antibody sAB-57 (grey) was employed as a crystallization chaperone and yielded essential crystal packing interactions. (**c**, **d**) The *S. cerevisiae* CNC crystal structure fitted into the negative-staining EM reconstructions of the *S. cerevisiae* (**c**) and human CNC (**d**). The CNC crystal structure and EM envelopes are illustrated in cartoon representation and grey transparent surfaces, respectively. Notably, additional density for the two human coat nucleoporins Nup37 and Nup43 is observed in the EM reconstruction of the human CNC. (**e**) The negative-staining EM structure of the isolated human CNC (also shown in **d**) and the tomographic map of the entire NPC were resolved to ~32 Å (EMDB 2444 and 2443) [3]. A systematic fitting analysis revealed that 32 copies of the CNC fit into sixteen-membered nucleoplasmic and cytoplasmic CNC rings (only one is shown fully) of the tomographic map (transparent gray). The fitting suggests the formation of two concentric, reticulated eight-membered rings on both the nucleoplasmic and cytoplasmic site of the NPC, in which the CNCs are arranged in a head-to-tail fashion. The outer (blue) and inner (green) CNC rings are rotated slightly with respect to each other. The nuclear envelope is illustrated in yellow. Image adapted from reference [3].

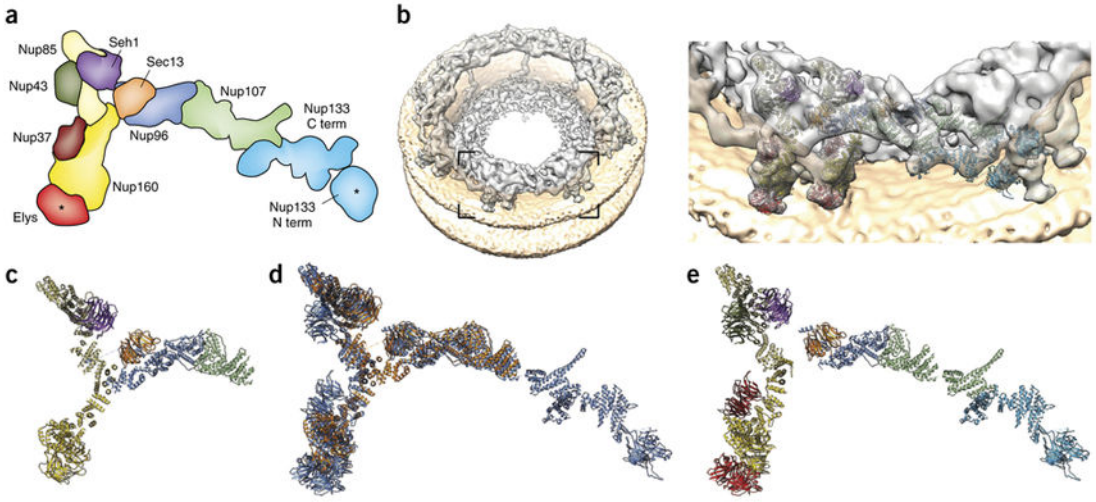

Figure 2. The structural organization of the coat nucleoporin complex (CNC) *in situ* is consistent with structural analysis *in vitro*

(**a**) Schematic representation of the vertebrate CNC indicating the position of all components. The human coat nucleoporins Nup160, Nup96, and Nup107 correspond to yeast coat nucleoporins Nup120, Nup145C, and Nup84 (Figure 1B), respectively. The human coat nucleoporins Nup43, Nup37, and Elys are absent in the *S. cerevisiae* CNC. Asterisks mark domains that can be confidently positioned due to available complementary data but not accurately oriented due to lack of structural data. (**b**) Tomographic map of the human NPC at a resolution of up to ~23 Å. The inset indicates a rotational segment of the nuclear ring that is magnified on the right with the fitted coat nucleoporin crystal structures shown in cartoon representation, colored according to (**a**). (**c**) Crystal structure of the *S. cerevisiae* CNC (lacking Nup133), the CNC model obtained by independent fitting of the individual coat nucleoporin crystal structures into the tomographic map, and their superposition. The same structure (orange) superimposed with a hybrid structure corresponding to (**d**; blue) that was obtained independently by fitting the individual X-ray structures into the tomographic map. Both structures shown in (**e**) were not fitted into each other but are shown superimposed based on the independent fits into the tomographic map. The superposition therefore effectively illustrates the accuracy of the present structural assignments. The image in (**a**) has been adapted from reference [35].

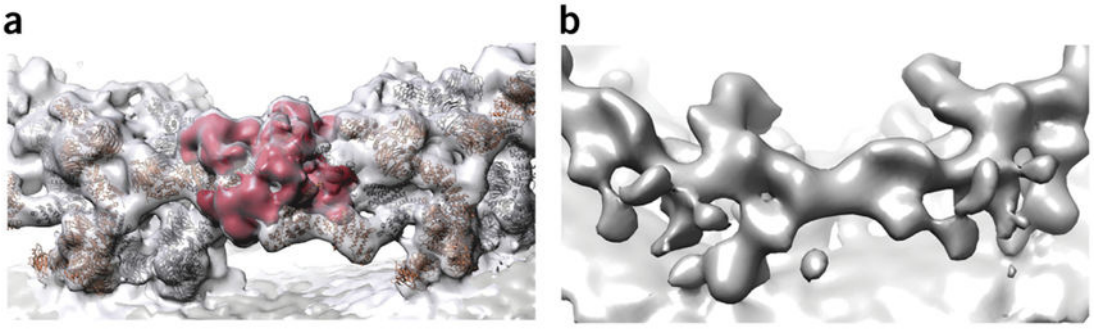

Figure 3. Gene Silencing of Nup358 causes loss of the outer CNC in the cytoplasmic ring

(**a**, **b**) Rotational segment (asymmetric unit) of the cytoplasmic ring of the human NPC obtained from a Nup358 gene silenced (**b**) and untreated condition (**a**, putative Nup358 density segmented in red). The electron optical density of the outer CNC is absent after gene silencing of Nup358 in case of the CR but not the NR (not shown). Images adapted from reference [35].

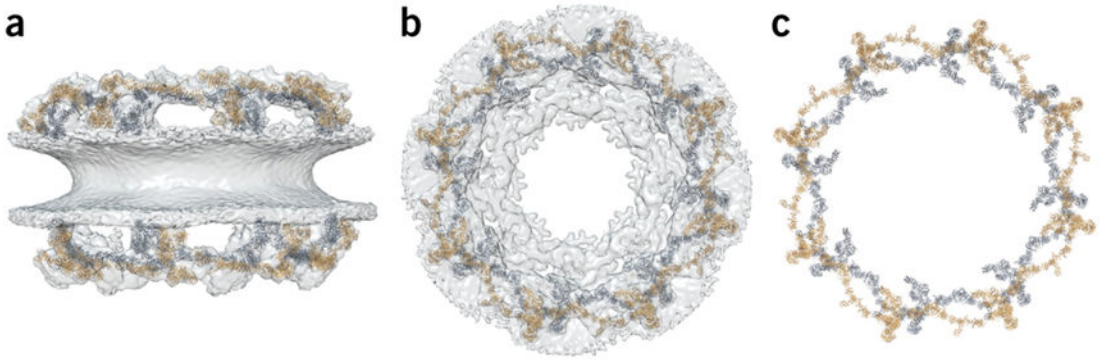

Figure 4. Schematic representation of the CNC arrangement in the intact NPC

Details as discussed in the text. (**a**) Side view of the nuclear pore as observed by cryo-EM; superposed with the inner (grey) and outer (orange) Y-complexes. (**b**) Same as (**a**) but in top view. (**c**) same as (**b**) but without any additional density.

Table 1
Fungi and vertebrate nucleoporin subcomplexes

Nucleoporins with multiple complex memberships are listed only once to make the list non-redundant. Additional binders that are not classified as nucleoporins, such as dyn2 (Nup159-complex) or RanGAP1-sumo1-ubc9 (Nup358 complex) are not listed. Nucleoporins with unclear subcomplex membership are listed under ‘others’. While multiple isoforms are separated with commas, alternative names are given in brackets.

Fungi	Vertebrates	Component
Coat nucleoporin complex (Y-complex)	*Nup107 complex*	
Nup120	Nup160	coat
	Nup37	coat
Ely-5	Elys	
Nup145C	Nup96	coat
Sec13	Sec13	coat
Nup85	Nup85	coat
Seh1	Seh1	coat
	Nup43	coat
Nup84	Nup107	coat
Nup133	Nup133	coat
Inner ring complex (Nic96 complex)	*Nup93 complex*	
Nup192	Nup205	adaptor
Nup188	Nup188	adaptor
Nup157, Nup170	Nup155	adaptor
Nic96	Nup93	adaptor
Nup53, Nup59	Nup35	
Nup145N, Nup116, Nup100	Nup98	
Nup159 complex (P-complex)	*Nup214 complex*	
Nup159	Nup214 (CAN)	cytoplasmic filament
Nup82	Nup88	cytoplasmic filament
Nsp1-complex (channel nucleoporin heterotrimer)	*Nup62 complex*	
Nsp1	Nup62	channel
Nup49	Nup58	channel
Nup57	Nup54	channel
	Nup358–RanGAP1-SUMO1-Ubc9 complex	
	Nup358 (RanBP2)	cytoplasmic filament
Others	*Others*	
	Aladin (AAAS)	

Fungi	Vertebrates	Component
Gle1	Gle1	
Rae1 (Gle2)	Rae1 (Gle2)	
Nup42	Nlp1 (hCG1)	
NDC1	NDC1	transmembrane
	POM121	transmembrane
	Gp210	transmembrane
POM152		transmembrane
POM34		transmembrane
Mlp1, Mlp2	Tpr	nuclear basket
Nup2	Nup50	nuclear basket
	Nup153	nuclear basket
Nup1		
Nup60		